Focusing of light in a three-dimensional cubic photonic crystal

J. Mizuguchi,[1] Y. Tanaka,[1] S. Tamura,[1] and M. Notomi[2]
[1]*Department of Applied Physics, Hokkaido University, Sapporo 060-8628, Japan*
[2]*NTT Basic Research Laboratories, Atsugi 243-0198, Japan*
(Received 5 July 2002; revised manuscript received 17 October 2002; published 27 February 2003)

The dielectric properties of photonic crystals are, in general, anisotropic spatially. This means that the constant-frequency surfaces of photons in wave-vector space are deformed from spherical shapes, leading to the photon focusing effects which are significantly enhanced at frequencies close to the photonic band gaps (PBG's). We find that the associated group-velocity surfaces of photons in real space are folded near PBG's and this gives rise to the appearance of photon caustics. We explicitly show these effects by illustrating theoretical images of photons transmitted through a photonic crystal. The calculation is made with the plane-wave-expansion method and numerical examples are given for a three-dimensional cubic lattice consisting of air and silicon.

DOI: 10.1103/PhysRevB.67.075109 PACS number(s): 42.70.Qs, 42.15.−i

I. INTRODUCTION

There has been a growing interest in recent years in fabricating photonic band-gap (PBG) structures or periodic, dielectric structures which exhibit a ''forbidden'' frequency region where electromagnetic waves cannot propagate along any direction.[1,2] These PBG structures, which are also called photonic crystals or photonic lattices, may bring about a variety of physical phenomena of both fundamental and practical interest. Three-dimensional (3D) crystals with PBG's in the visible and infrared frequency regimes, which are expected to provide the most effective potential in applications, have very recently been fabricated and measurements of the photon transmission are reported.[3]

The dielectric properties of photonic crystals which are composite systems of different optical properties are anisotropic in general. As far as the ''photon images'' we will consider are concerned, however, this anisotropy does not have a large effect for photons at low frequencies. In contrast, the effect is considerably enhanced at frequencies close to the Brillouin zone boundaries or PBG's. Here we note that the energy transport of photons in photonic crystals is governed by their group velocities ($\mathbf{V}_g = \partial\omega/\partial\mathbf{k}$ with ω an angular frequency and $\mathbf{k}$ a wave vector) that are deeply related to the shapes of the constant-frequency surfaces (ω surfaces) of photons in wave-vector space ($\mathbf{k}$ space).[4,5] Owing to the presence of the dielectric anisotropy, the ω surfaces of photons in photonic crystals should be deformed from a spherical shape and hence the distribution of the photon group velocities in real space is not uniform even if the wave vectors $\mathbf{k}$ are distributed uniformly in $\mathbf{k}$ space. This will lead to the focusing and defocusing of photons in the photonic crystals which are enhanced by increasing the frequency.

A related example is the spatial anisotropy of the enhanced optical gain[6] and so-called a superprism effect[7] reported recently. In the latter the angle of light deflected in a bulk crystal is typically about $\delta\theta = 0.1°$ for a small change of the wavelength, $\delta\lambda/\lambda = 0.1\%$. However, in some cases this is enhanced up to about $\delta\theta = 50°$. This enhancement is caused by the fact that the direction of the group velocity is given by the outward normal of the ω surface of photons and accordingly very sensitive to the deformation of the ω surfaces. Thus the superprism effect occurs when we compare the group-velocity directions by changing the photon frequencies for a given wave-vector direction.

Another interesting effect is the one which should occur when we compare the group-velocity directions by scanning the wave-vector directions with a given photon frequency. This is related to the question of how the energy of ballistic photons is transported in photonic crystals when they are emitted from a point source in a wide range of directions. The answer is determined by the geometrical structures of the entire ω surfaces of photons in the Brillouin zone. Experimentally this should be understood by studying photon images analogous to the phonon images in the bulk and also composite structures.[8] The phonon image is a 2D map of the acoustic phonon intensity (i.e., phonon energy carried by the group velocity) at a sample surface that is obtained when phonons are excited at a point source of the opposite face.

Here we remark that the spatial distribution of the phonon group velocities in a crystalline solid is highly anisotropic and the focusing and defocusing of ballistically propagating phonons have been observed experimentally.[9] In particular, the phonon imaging method made a substantial contribution to revealing how acoustic energy emanating from a point source is distributed in a crystal lattice.[8,10] A similar photon imaging technique would be utilized for the experimental verification of the PBG's, which has so far been made by measuring the transmission dip of photons in a given propagation direction.

The purpose of the present work is to elucidate theoretically ballistic photon propagation in 3D photonic crystals. Specifically, we consider the case where monochromatic photons are emitted from a point source inside or outside the photonic crystal randomly in the wave-vector directions and study the resulting group-velocity (or energy) distribution in the photonic crystal. In particular, we show how the deformation of the constant-frequency surface of photons in the first Brillouin zone affects the optical energy transport in the photonic crystals as the frequency changes. The results are presented as theoretical photon images (spatial maps of the

photon group velocities) which display the distribution of photons in the (100) plane of a cubic 3D photonic crystal.

In Sec. II we develop the mathematical formulation for determining photon group velocities in a 3D cubic photonic crystal. Numerical examples for the photon images are given in Sec. III for an air/Si lattice for various photon frequencies. The implications of our results are discussed in Sec. IV.

II. FORMULATION

The band structures of photons are obtained by solving Maxwell's equations

$$\nabla \times \mathbf{E}(\mathbf{r},t) = -\mu_0 \frac{\partial}{\partial t}\mathbf{H}(\mathbf{r},t), \tag{1}$$

$$\nabla \times \mathbf{H}(\mathbf{r},t) = \varepsilon_0 \varepsilon(\mathbf{r}) \frac{\partial}{\partial t}\mathbf{E}(\mathbf{r},t), \tag{2}$$

where $\mathbf{r}=(x,y,z)$, $\mathbf{E}(\mathbf{r},t)$ and $\mathbf{H}(\mathbf{r},t)$ are the electric and magnetic fields, and μ_0 and ε_0 are the magnetic permeability and permittivity of a free space. In a spatially modulated system, the dielectric constant ε depends on the position $\mathbf{r}$, i.e., $\varepsilon=\varepsilon(\mathbf{r})$. Here we assume the harmonic time dependence $\mathbf{E}(\mathbf{r},t)=\mathbf{E}(\mathbf{r})\exp(-i\omega t)$ and $\mathbf{H}(\mathbf{r},t)=\mathbf{H}(\mathbf{r})\exp(-i\omega t)$ for both the electric and magnetic fields. Equations (1) and (2) should be supplemented with

$$\nabla \cdot [\varepsilon(\mathbf{r})\mathbf{E}(\mathbf{r})] = 0, \tag{3}$$

$$\nabla \cdot \mathbf{H}(\mathbf{r}) = 0. \tag{4}$$

Thus, we have to solve the wave equation

$$\nabla \times \nabla \times \mathbf{E}(\mathbf{r}) = \left(\frac{\omega}{c}\right)^2 \varepsilon(\mathbf{r})\mathbf{E}(\mathbf{r}) \tag{5}$$

or equivalently

$$\nabla \times [\varepsilon(\mathbf{r})^{-1} \nabla \times \mathbf{H}(\mathbf{r})] = \left(\frac{\omega}{c}\right)^2 \mathbf{H}(\mathbf{r}), \tag{6}$$

where c is the light velocity in vacuum.

In order to solve Eq. (5) or (6) we employ the plane-wave-expansion scheme.[11–14] First we expand the dielectric constant as

$$\varepsilon(\mathbf{r}) = \sum_{n=1}^{N} \varepsilon(\mathbf{G}_n)\exp(i\mathbf{G}_n \cdot \mathbf{r}), \tag{7}$$

where N is the number of plane waves in the truncated Fourier series expansion and $\varepsilon(\mathbf{G}_n)$ is a Fourier coefficient with $\mathbf{G}_n$ a reciprocal lattice vector. Similarly, we have to expand the electric or magnetic field. Here we note that Eq. (6) contains a derivative of the dielectric constant $\varepsilon(\mathbf{r})$ that changes abruptly at the boundary between the constituent materials of the photonic crystals, so the convergence of the magnetic field should be much slower than the electric field. Accordingly, we consider Eq. (5) and expand the electric field as (this means that we employ the so-called E method)

$$\mathbf{E}(\mathbf{r}) = \sum_{n=1}^{N} \mathbf{E}(\mathbf{G}_n)\exp[i(\mathbf{k}+\mathbf{G}_n)\cdot \mathbf{r}], \tag{8}$$

where $\mathbf{E}(\mathbf{G}_n)$ are Fourier coefficients and $\mathbf{k}$ is a 3D Bloch wave vector. Now we introduce N-component column vectors $\overline{\mathbf{E}}_{(i)}$ and diagonal matrices $\overline{K}_i$ $(i=x,y,z)$ with $N\times N$ elements defined by

$$\overline{\mathbf{E}}_{(i)} = \begin{pmatrix} E_i(\mathbf{G}_1) \\ E_i(\mathbf{G}_2) \\ E_i(\mathbf{G}_3) \\ \vdots \\ E_i(\mathbf{G}_N) \end{pmatrix}, \tag{9}$$

$$\overline{K}_i = \begin{pmatrix} (\mathbf{k}+\mathbf{G}_1)_i & 0 & 0 & \cdots & 0 \\ 0 & (\mathbf{k}+\mathbf{G}_2)_i & 0 & \cdots & 0 \\ 0 & 0 & (\mathbf{k}+\mathbf{G}_3)_i & \cdots & 0 \\ \vdots & \vdots & \vdots & \ddots & \vdots \\ 0 & 0 & 0 & \cdots & (\mathbf{k}+\mathbf{G}_N)_i \end{pmatrix}. \tag{10}$$

We further define an $N\times N$ matrix $\overline{\varepsilon}=(\overline{\varepsilon}_{nm})$ with $\overline{\varepsilon}_{nm} \equiv \varepsilon(\mathbf{G}_n-\mathbf{G}_m)$ and a $3N$-component column vector $\tilde{\mathbf{E}}$ with

$$\tilde{\mathbf{E}} = \begin{pmatrix} \overline{\mathbf{E}}_{(x)} \\ \overline{\mathbf{E}}_{(y)} \\ \overline{\mathbf{E}}_{(z)} \end{pmatrix}. \tag{11}$$

Substituting these equations into Eq. (5), we have

$$\left[M - \left(\frac{\omega}{c}\right)^2 D\right]\tilde{\mathbf{E}} = 0, \tag{12}$$

where

$$M = \begin{pmatrix} \overline{K}_y^2+\overline{K}_z^2 & -\overline{K}_x\overline{K}_y & -\overline{K}_x\overline{K}_z \\ -\overline{K}_x\overline{K}_y & \overline{K}_x^2+\overline{K}_z^2 & -\overline{K}_y\overline{K}_z \\ -\overline{K}_x\overline{K}_z & -\overline{K}_y\overline{K}_z & \tilde{K}_x^2+\overline{K}_y^2 \end{pmatrix} \tag{13}$$

and

$$D = \begin{pmatrix} \overline{\varepsilon} & 0 & 0 \\ 0 & \overline{\varepsilon} & 0 \\ 0 & 0 & \overline{\varepsilon} \end{pmatrix} \tag{14}$$

are $3N\times 3N$ matrices. The dispersion relation of photons $\omega=\omega(\mathbf{k})$ is obtained from Eq. (12). The group velocities of photons, $\mathbf{V}_g=\partial\omega/\partial\mathbf{k}$, is calculated as follows: First we note that

$$\tilde{\mathbf{E}}^{\dagger}\left[M-\left(\frac{\omega}{c}\right)^2 D\right]\tilde{\mathbf{E}}=0. \tag{15}$$

Then differentiating Eq. (15) with respect to $\mathbf{k}$, we have

$$\frac{\partial\tilde{\mathbf{E}}^{\dagger}}{\partial\mathbf{k}}\left[M-\left(\frac{\omega}{c}\right)^2 D\right]\tilde{\mathbf{E}}+\tilde{\mathbf{E}}^{\dagger}\left[\frac{\partial M}{\partial\mathbf{k}}-\frac{2\omega}{c^2}\frac{\partial\omega}{\partial\mathbf{k}}D\right]\tilde{\mathbf{E}}+\tilde{\mathbf{E}}^{\dagger}\left[M-\left(\frac{\omega}{c}\right)^2 D\right]\frac{\partial\tilde{\mathbf{E}}}{\partial\mathbf{k}}=0. \tag{16}$$

From this equation we find

$$\mathbf{V}_g=\frac{\partial\omega}{\partial\mathbf{k}}=\frac{c^2}{2\omega}\frac{\tilde{\mathbf{E}}^{\dagger}\frac{\partial M}{\partial\mathbf{k}}\tilde{\mathbf{E}}}{\tilde{\mathbf{E}}^{\dagger}D\tilde{\mathbf{E}}}. \tag{17}$$

With the condition (3) or

$$\bar{K}_x\bar{\varepsilon}\bar{\mathbf{E}}_{(x)}+\bar{K}_y\bar{\varepsilon}\bar{\mathbf{E}}_{(y)}+\bar{K}_z\bar{\varepsilon}\bar{\mathbf{E}}_{(z)}=0, \tag{18}$$

$\bar{\mathbf{E}}_{(y)}$ is written in terms of $\bar{\mathbf{E}}_{(x)}$ and $\bar{\mathbf{E}}_{(z)}$, and Eq. (12) is reduced to

$$\begin{pmatrix} \bar{K}_y^2+\bar{K}_z^2+\bar{K}_y\bar{K}_x\bar{\varepsilon}^{-1}\bar{K}_y^{-1}\bar{K}_x\bar{\varepsilon} & \bar{K}_y\bar{K}_x\bar{\varepsilon}^{-1}\bar{K}_y^{-1}\bar{K}_z\bar{\varepsilon}-\bar{K}_z\bar{K}_x \\ \bar{K}_y\bar{K}_z\bar{\varepsilon}^{-1}\bar{K}_y^{-1}\bar{K}_x\bar{\varepsilon}-\bar{K}_x\bar{K}_z & \bar{K}_x^2+\bar{K}_y^2+\bar{K}_y\bar{K}_z\bar{\varepsilon}^{-1}\bar{K}_y^{-1}\bar{K}_z\bar{\varepsilon} \end{pmatrix}\begin{pmatrix}\bar{\mathbf{E}}_{(x)}\\ \bar{\mathbf{E}}_{(z)}\end{pmatrix}=\left(\frac{\omega}{c}\right)^2\begin{pmatrix}\bar{\varepsilon} & 0\\ 0 & \bar{\varepsilon}\end{pmatrix}\begin{pmatrix}\bar{\mathbf{E}}_{(x)}\\ \bar{\mathbf{E}}_{(z)}\end{pmatrix}. \tag{19}$$

Equation (19) should be solved for the photonic lattice specified.[15]

III. NUMERICAL RESULTS

We present numerical results for a 3D cubic lattice composed of materials with $\varepsilon_a=\varepsilon_{\text{air}}=1$ (air) and $\varepsilon_b=\varepsilon_{\text{Si}}=12.96$ (silicon). The structure of a unit cell is shown in Fig. 1. This is the same as the building block of the simple cubic lattice considered by Sözüer and Haus[16] and actually fabricated by Lin *et al.*[3] The expressions of $\varepsilon(\mathbf{G}_n)$ for the cubic lattice considered are given in the Appendix.

The dispersion relations of photons in the Γ-X direction and also along the Brillouin-zone boundary X-M-R of this crystal with a filling fraction [f defined by Eq. (A7)] $f=0.19$ (with $b/a=0.28$) are shown in Fig. 2 together with

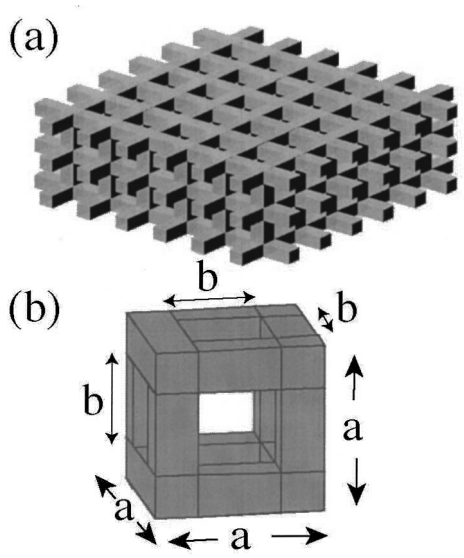

FIG. 1. (a) Schematic of the three-dimensional cubic photonic crystal. (b) A unit building block of (a).

the density of states (DOS). In the calculation of these dispersion curves the number of plane waves kept in the expansions (7) and (8) are $N=7^3=343$. More precisely, as the reciprocal lattice vectors $\mathbf{G}_n$ ($n=1-N$) in the simple cubic crystal introduced in Sec. II, we choose $\mathbf{G}_n=2\pi(n_x,n_y,n_z)/a\equiv(G_{nx},G_{ny},G_{nz})$ with $-3\leqslant n_x,n_y,n_z\leqslant 3$. The convergence of the calculation with this number of plane waves has been checked by the fact that no appreciable change has been seen even if we increase the number of plane waves further. We have also confirmed that the dispersion curves obtained are identical to the ones previously obtained by Sözüer and Haus[16] and also by Lin *et al.*[3] However, the DOS we have obtained is more smooth than the one illustrated by Sözüer and Haus and clearly shows, in addition to several van Hove singularities, the existence of a complete gap at frequencies around the normalized frequency of $\tilde{\omega}\equiv\omega a/2\pi c=0.37$. This is because, in our calculation of the DOS, we have employed an accurate linear analytic method for the Brillouin-zone integration devised by Gilat and Raubenheimer.[17] In this calculation we have used a uniform shifted mesh over the irreducible section of the first Brillouin zone and the number of intervals into which we have subdivided the longest Γ-X axis is 50. In Ref. 16, however, a simple root-sampling method with 300 $\mathbf{k}$ points in the Brillouin zone has been used.

At the X point of the Brillouin-zone boundary the forbidden frequency gap is considerably large, extending from $\tilde{\omega}=0.25$ up to the complete gap. In the present calculation we concentrate our attention on the frequency region below the lowest complete gap and select eight frequencies $\tilde{\omega}=\tilde{\omega}_1-\tilde{\omega}_8$ ($\tilde{\omega}_1=0.15$, $\tilde{\omega}_2=0.22$, $\tilde{\omega}_3=0.25$, $\tilde{\omega}_4=0.27$, $\tilde{\omega}_5=0.29$, $\tilde{\omega}_6=0.30$, $\tilde{\omega}_7=0.34$, and $\tilde{\omega}_8=0.37$) for illustration.

Now we display the photon images primarily determined from the shapes of the constant-frequency surfaces calculated from the dispersion curves. These images are constructed by randomly distributing a large number of photon wave vectors whose directions are assumed to be uniform in wave-vector space. For each wave vector of a photon the

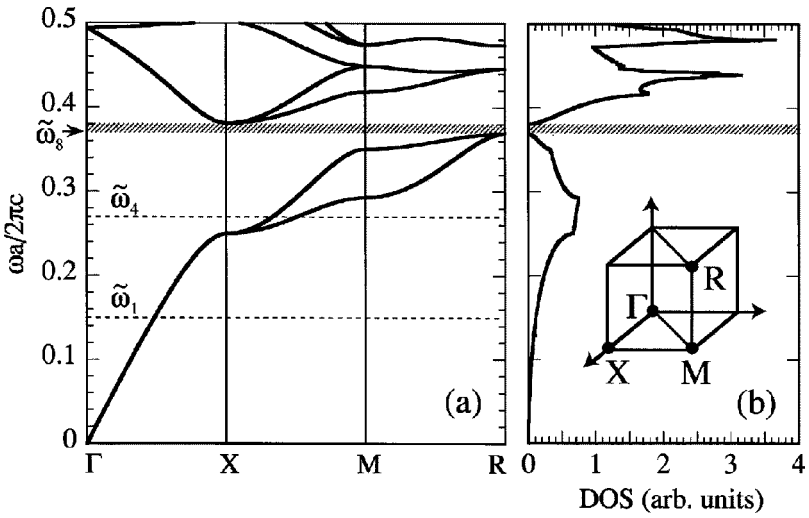

FIG. 2. (a) Dispersion relations of photons in the cubic air/silicon photonic crystal (Fig. 1) along the boundary of the irreducible part of the Brillrouin zone shown in the inset of (b). Filling fraction assumed is $f=0.19$. Normalized frequencies $\omega a/2\pi c \equiv \tilde{\omega} = \tilde{\omega}_1 = 0.15$, $\tilde{\omega} = \tilde{\omega}_4 = 0.27$, and $\tilde{\omega} = \tilde{\omega}_8 = 0.37$ are indicated. (b) Density of states calculated with the linear analytic method.

corresponding group velocity direction is calculated and the point of its intersection with the (001) plane separated a distance L from the photon source is recorded irrespective of the magnitude of the group velocity. This detection plane of $3L \times 3L$ in size is then divided into 150×150 square grids and the number of group velocity vectors involved inside each grid is counted and multiplied by the photon frequency. These numbers are then normalized and displayed in a gray scale, resulting in a photon image.

Thus, the photon images in the cubic plane (x-y plane) at $\tilde{\omega} = \tilde{\omega}_1$ and $\tilde{\omega} = \tilde{\omega}_4$ are plotted in Figs. 3(a) and 3(b), respectively, for the square region $-1.5 < x/L,\ y/L < 1.5$. At $\tilde{\omega} = \tilde{\omega}_1$ (this is a representative of low photon frequencies), the image is almost isotropic: that is, the intensity distribution exhibits the angular dependence expected from the Lambert cosine law. More explicitly, the normalized intensity profile coincides well with the formula $\cos[\tan^{-1}(x/L)]/[1+(x/L)^2]$ illustrated by the dashed line in Fig. 3(c) and no noticeable feature can be seen. However, the image of Fig. 3(b) at $\tilde{\omega} = \tilde{\omega}_4$ (this frequency is found inside the gap in the Γ-X (the [100]) direction) is quite anisotropic. Also a remarkable feature found in this photon image is the presence of the central region surrounded by a circular high-intensity line of radius about $\sim L$, where photon transmission is very small. This is evidently caused by the presence of frequency gaps in the [100] and its equivalent directions.

To allocate the origin of the characteristic structures in the photon images predicted, here we study the behaviors of photons at frequencies $\tilde{\omega} = \tilde{\omega}_1$ and $\tilde{\omega} = \tilde{\omega}_4$ more in detail. At the former frequency the wavelengths of photons are much longer than the lattice constant a and the present photonic-band-gap structure with cubic symmetry exhibits an isotropic dielectric property as shown by Datta *et al.* in the limit of $|\mathbf{k}| \to 0$.[18] Figure 4 exhibits the sections of the constant-

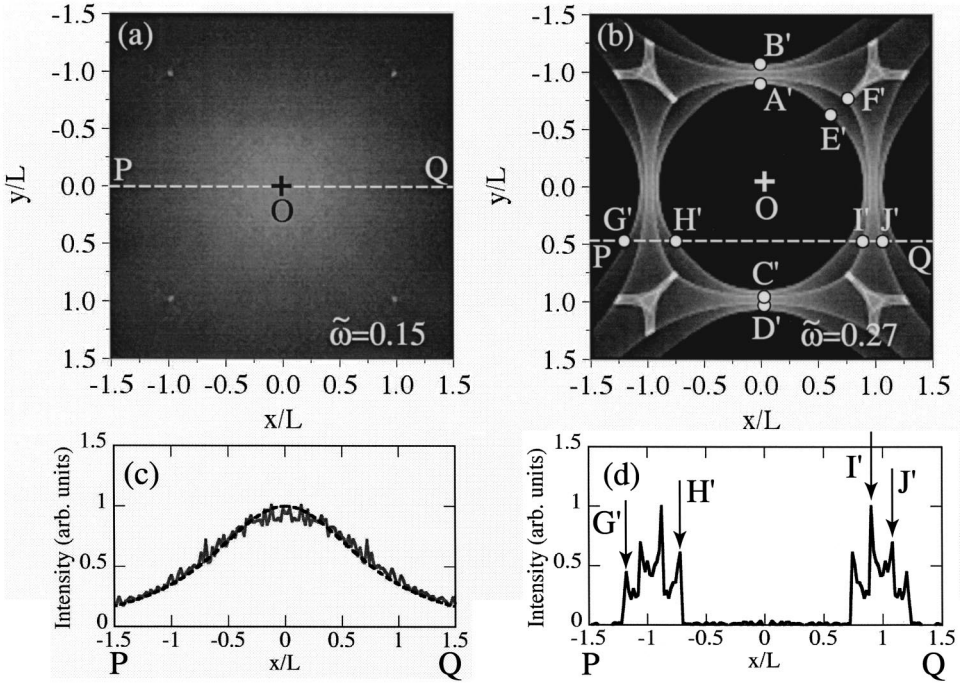

FIG. 3. Theoretical photon images (brightness corresponds to photon intensity) on the (001) plane at (a) $\tilde{\omega} = \tilde{\omega}_1 = 0.15$ and (b) $\tilde{\omega} = \tilde{\omega}_4 = 0.27$. (c) Photon intensity along the horizontal line PQ in (a). The dashed line shows $\cos[\tan^{-1}(x/L)]/[1+(x/L)^2]$ (the Lambert formula). (d) Photon intensity along the horizontal line PQ in (b). The intensity peaks occur at the outer (inner) caustics G' and H' (I' and J') in the focusing structure of (b).

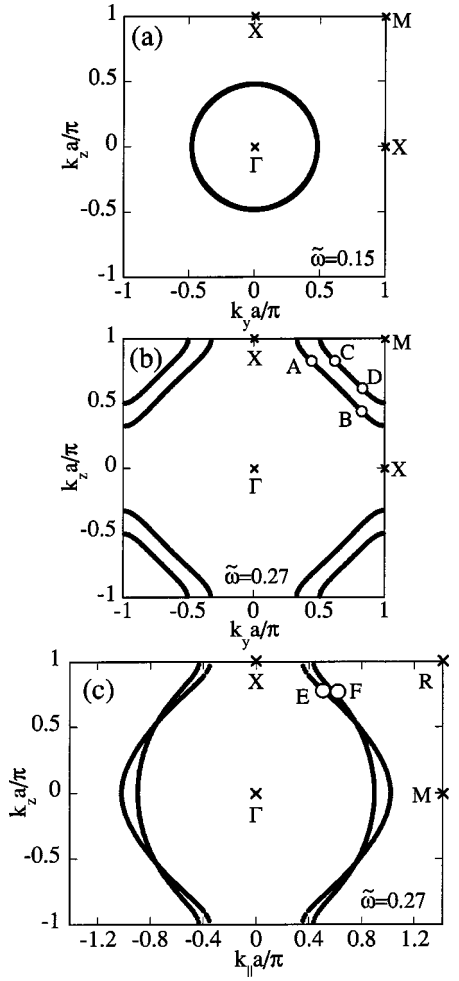

FIG. 4. (a) The sections of the constant-frequency surfaces in the first Brillouin zone by the (100) plane at $\tilde{\omega}=\tilde{\omega}_1=0.15$. Two curves almost overlap. (b) The sections of the constant-frequency surfaces by the (100) plane at $\tilde{\omega}=\tilde{\omega}_4=0.27$. The points labeled $A-D$ are the inflection points on the constant-frequency curves. (c) The sections of the constant-frequency surfaces by the (110) plane at $\tilde{\omega}=\tilde{\omega}_4=0.27$. The points labeled E and F are the inflection points on these curves.

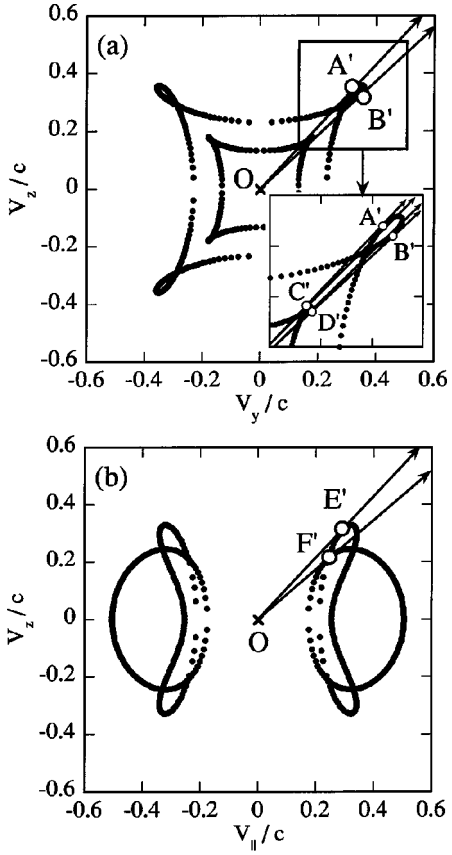

FIG. 5. (a) The group-velocity curves corresponding to the constant-frequency curves of Fig. 4 (b) at $\tilde{\omega}=\tilde{\omega}_4=0.27$. The points labeled $A'-D'$ define the caustics [A' and B' on the (001) plane are indicated in Fig. 3(b)] originating from the inflection points $A-D$ on the constant-frequency curves. (b) The group-velocity curves corresponding to the constant-frequency curves of Fig. 4(c) at $\tilde{\omega}=\tilde{\omega}_4=0.27$. The points labeled E' and F' are the caustics [E' and F' on the (001) plane are indicated in Fig. 3(b)] originating from the inflection points E and F on the constant-frequency curves. To generate these curves, the wave-vector directions are assumed to be distributed uniformly (every 2°) on the constant-frequency curves. So the local density of points in each curve measures the focusing of photons in a given direction.

frequency surfaces by the (100) plane at $\tilde{\omega}=\tilde{\omega}_1$ in the first Brillouin zone. We see that at this frequency the constant-frequency surfaces of photons are almost degenerate (with approximately spherical shapes) and entirely located inside the first zone. So the group velocities are also distributed nearly isotropically in real space and no specific feature is expected in the energy propagation of photons.

In contrast, at $\tilde{\omega}=\tilde{\omega}_4$ the constant-frequency surfaces are no longer degenerate and exhibit significant anisotropy. In addition, they are partly cut off by the Brillouin-zone boundaries because this frequency is found inside the forbidden gap for a finite range of the propagation direction around the [100] and its equivalent directions. Figures 4(b) and 4(c) display the sections of the constant-frequency surfaces by the (100) and (110) planes at $\tilde{\omega}=\tilde{\omega}_4$. These constant-frequency curves are deformed markedly from circular shapes and mutually disconnected. Associated with these deformations the inflection points $A-F$ appear on the constant-frequency curves (corresponding to parabolic lines with zero Gaussian curvature on the constant-frequency surfaces), leading to a folding of the group-velocity curves of photons.

The (100) and (110) sections of the group-velocity curves calculated from the constant-frequency curves of Figs. 4(b) and 4(c) are shown in Figs. 5(a) and 5(b), respectively. In these figures the group-velocity curves are folded at the points labeled $A'-F'$ corresponding to the inflection points $A-F$ on the constant-frequency curves. These points $A'-F'$ are called caustics along which the intensity of photons becomes infinite in the geometrical optics approximation.

Finally, we show in Fig. 6 the photon images obtained as we increase the frequency consecutively from $\tilde{\omega}=\tilde{\omega}_1=0.15$ to $\tilde{\omega}=\tilde{\omega}_8=0.37$ (inside the complete gap). We see how caustic lines (focusing singularities) appear as the frequency increases in the images and how they are deformed and eventually the photon transmission is prohibited.

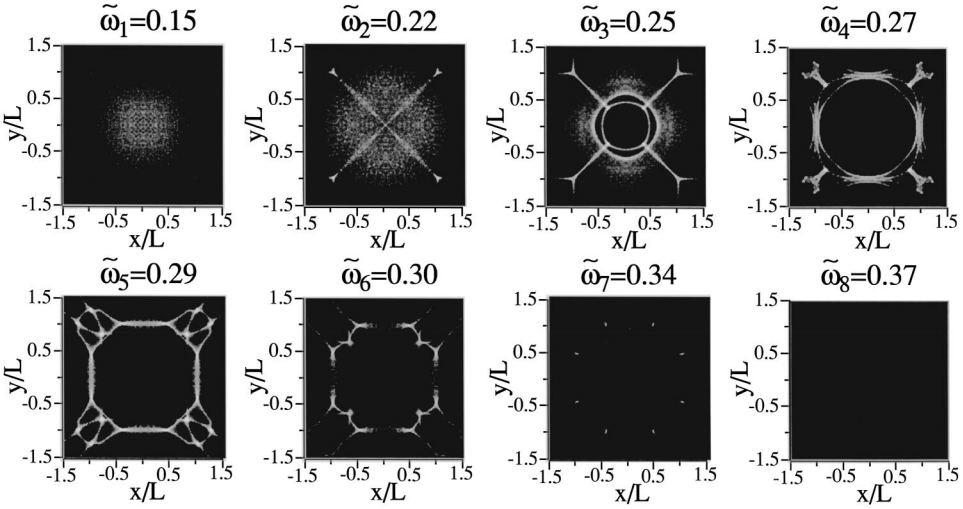

FIG. 6. Calculated photon images on the (001) plane at eight consective frequencies $\tilde{\omega}=\tilde{\omega}_1=0.15$, $\tilde{\omega}_2=0.22$, $\tilde{\omega}_3=0.25$, $\tilde{\omega}_4=0.27$, $\tilde{\omega}_5=0.29$, $\tilde{\omega}_6=0.30$, $\tilde{\omega}_7=0.34$, and $\tilde{\omega}_8=0.37$.

IV. CONCLUDING REMARKS

In the present work we have theoretically studied photon focusing in a cubic 3D photonic crystal consisting of air and Si. The dielectric anisotropy of this composite system, which depends on frequency, leads to a concentration of the energy of photons along specific directions even if they are emitted isotropically (in wave-vector space) in the photonic crystal. More explicitly, we have shown that the presence of PBG's greatly enhances the anisotropic photon propagation in the crystal through the deformation of the constant-frequency surfaces near the Brillouin-zone boundaries. These new predictions should be verified by a photon imaging experiment analogous to photon imaging experiments[8,10] in which the global angular distribution of the ballistic energy propagation of photons may be measured on the whole surface of a photonic crystal. It should be noted that experimental verification of the PBG's has so far been made only locally, that is, by measuring the transmission dips of photons in a given propagation direction. Here we also remark that along those strong focusing directions of photons their nonlinear effects are expected to be significantly increased.

The present calculation is based on the dispersion relations of photons valid in an infinite lattice. Real photonic crystals fabricated are, of course, finite in size and have surfaces. In measuring photon energies, those of photons reflected at the crystal surfaces will be superimposed onto the energies photons emitted primarily from the point source and hence may affect the photon images. Thus, there should be an additional contribution to the images of photons caused by single and multiple reflections at the surfaces of a photonic crystal. This would be a topic to be studied separately. Also similar analyses for photonic crystals with more complicated lattice structures, such as face-centered-cubic and diamond structures (for which wider PBG's are expected), would be interesting.

ACKNOWLEDGMENTS

We are grateful to Dr. N. Hatakenaka for stimulating discussions. The work at Hokkaido University was supported in part by a Grant-in-Aid for Scientific Research from the Ministry of Education, Science and Culture of Japan (Grant Nos. 09640385 and 14750045).

APPENDIX

In this appendix we give the expressions of $\varepsilon(\mathbf{G}_n)$ for the cubic lattice we consider. First, we note that

$$\varepsilon(\mathbf{r})=\varepsilon_b+(\varepsilon_a-\varepsilon_b)S(\mathbf{r}), \tag{A1}$$

where ε_a and ε_b are the dielectric constants of the matrix (Si) and background (air) materials, respectively, and $S(\mathbf{r})$ takes either unity or zero depending on whether the position $\mathbf{r}$ is inside (unity) or outside (zero) silicon. Thus, inverting Eq. (7), we have

$$\varepsilon(\mathbf{G}_n)=\varepsilon_b\delta_{G_n,0}+\frac{1}{V_0}(\varepsilon_a-\varepsilon_b)\int_{V_0}S(\mathbf{r})\exp(-i\mathbf{G}_n\cdot\mathbf{r})d\mathbf{r}, \tag{A2}$$

with $V_0=a^3$ a unit cell volume. The reciprocal lattice vector $\mathbf{G}_n$ in the simple cubic lattice is given by $\mathbf{G}_n=2\pi(n_x,n_y,n_z)/a\equiv(G_{nx},G_{ny},G_{nz})$, where (n_x,n_y,n_z) is a set of integers. Then Eq. (A2) can be calculated explicitly and the resulting expression is

$$\varepsilon(\mathbf{G}_n)=\frac{-16(\varepsilon_a-\varepsilon_b)}{V_0}\frac{1}{G_{nx}G_{ny}G_{nz}}\times\sin\left(\frac{b}{2}G_{nx}\right)\sin\left(\frac{b}{2}G_{ny}\right)\sin\left(\frac{b}{2}G_{nz}\right), \tag{A3}$$

for $G_{nx}\neq0$, $G_{ny}\neq0$, $G_{nz}\neq0$,

$$\varepsilon(\mathbf{G}_n)=\frac{4(\varepsilon_a-\varepsilon_b)(a-2b)}{V_0}\frac{1}{G_{nx}G_{ny}}\sin\left(\frac{b}{2}G_{nz}\right)\sin\left(\frac{b}{2}G_{ny}\right), \tag{A4}$$

for $G_{nx}\neq0$, $G_{ny}\neq0$, $G_{nz}=0$,

$$\varepsilon(\mathbf{G}_n)=\frac{4(\varepsilon_a-\varepsilon_b)(a-b)b}{V_0}\frac{1}{G_{nx}}\sin\left(\frac{b}{2}G_{nx}\right), \tag{A5}$$

for $G_{nx} \neq 0$, $G_{ny}=0$, $G_{nz}=0$, and

$$\varepsilon(0)=\varepsilon_b+(\varepsilon_a-\varepsilon_b)f, \tag{A6}$$

with the filling fraction f of air defined by

$$f=\frac{b^2(3a-2b)}{a^3}, \tag{A7}$$

where b is a side length of the air column inside the unit cell shown in Fig. 1(b).

[1] *Photonic Band Gaps and Localization*, edited by C. M. Soukoulis (Plenum, New York, 1993).

[2] J. D. Joannopoulos, R. D. Meade, and J. N. Winn, *Photonic Crystals* (Princeton University Press, Princeton, 1995).

[3] S.-Y. Lin *et al.*, J. Opt. Soc. Am. B **18**, 32 (2001).

[4] P. St. J. Russell, T. A. Birks, and F. D. Lloyd-Lucas, *Confined Electrons and Photons*, Vol. 340 of *NATO Advanced Study Institute, Series B: Physics*, edited by E. Burstein and C. Weisbuch (Plenum, New York, 1995), p. 585.

[5] M. Notomi, Phys. Rev. B **62**, 10 696 (2000).

[6] S. Nojima, Jpn. J. Appl. Phys., Part 2 **37**, L565 (1998); Jpn. J. Appl. Phys., Part 1 **37**, 6418 (1998).

[7] H. Kosaka *et al.*, Phys. Rev. B **58**, R10 096 (1998); Appl. Phys. Lett. **74**, 1370 (1999).

[8] J. P. Wolfe, *Imaging Phonons* (Cambridge University Press, Cambridge, England, 1998), Chap. 2.

[9] B. Taylor, H. J. Maris, and C. Elbaum, Phys. Rev. Lett. **23**, 416 (1969); Phys. Rev. B **3**, 1462 (1971).

[10] G. A. Northrop and J. P. Wolfe, *Nonequilibrium Phonon Dynamics* (Plenum, New York, 1985), Chap. 5.

[11] S. Satpathy, Z. Zhang, and M. R. Salehpour, Phys. Rev. Lett. **64**, 1239 (1990).

[12] K. M. Leung and Y. F. Liu, Phys. Rev. B **41**, 10 188 (1990); Phys. Rev. Lett. **65**, 2646 (1990).

[13] Z. Zhang and S. Satpathy, Phys. Rev. Lett. **65**, 2650 (1990).

[14] K. M. Ho, C. T. Chan, and C. M. Soukoulis, Phys. Rev. Lett. **65**, 3152 (1990).

[15] T. Suzuki and K. L. Yu, J. Opt. Soc. Am. B **12**, 804 (1995).

[16] H. S. Sözüer and J. W. Haus, J. Opt. Soc. Am. B **10**, 296 (1993).

[17] G. Gilat and L. Raubenheimer, Phys. Rev. **144**, 390 (1966).

[18] S. Datta, C. T. Chan, K. M. Ho, and C. M. Soukoulis, Phys. Rev. B **48**, 14 936 (1993).